JOURNAL OF EXPERIMENTAL ZOOLOGY 307A:145–155 (2007)

Architectural Gear Ratio and Muscle Fiber Strain Homogeneity in Segmented Musculature

EMANUEL AZIZI* AND ELIZABETH L. BRAINERD†
Department of Biology and Program in Organismic and Evolutionary Biology, University of Massachusetts, Amherst, Massachusetts 01003

ABSTRACT In the segmented axial musculature of fishes and amphibians, the patterns of muscle fiber shortening depend on both the orientation of muscle fibers relative to the long axis of the body as well as the distance of fibers from the neutral axis of bending (vertebral column). In this study we use the relatively simple architecture of salamander hypaxial muscles to explore the separate and combined effects of these morphological features on muscle fiber strains during swimming. In *Siren lacertina* the external oblique (EO) muscle has more obliquely oriented muscle fibers and is located further from the neutral axis of bending than the internal oblique (IO) muscle. To examine the effect of muscle fiber angle on strain patterns during swimming, we used sonomicrometry to quantify architectural gear ratio (AGR = longitudinal strain/fiber strain) in these two hypaxial muscles. By comparing the muscle fiber strains and shortening velocities of the EO and IO during swimming, we test whether variation in mediolateral position of the muscle layers is counteracted by their differences in AGR. We find that despite substantial differences in mediolateral position, the EO and IO undergo similar fiber strains and shortening velocities for a given amount of axial bending. Our results show that variation in muscle fiber angle acts to counteract differences in mediolateral position, thereby minimizing variation in muscle fiber strain and shortening velocity during swimming. These results highlight the significance of both muscle architecture and muscle moment arms in determining the fiber strains required for a given movement. *J. Exp. Zool. 307A:145–155, 2007.*

How to cite this article: Azizi E, Brainerd EL. 2007. Architectural gear ratio and muscle fiber strain homogeneity in segmented musculature. J. Exp. Zool. 307A:145–155.

At the sarcomere level, all vertebrate skeletal muscle fibers operate under a similar set of constraints. Maximal tension can only be generated over a limited range of muscle fiber strains and peak power is only possible over a specific range of shortening velocities. To optimize muscle performance, muscle fibers of the same fiber type recruited for a given task would be expected to have similar strains and shortening velocities in order to function within the optimal portions of the length–tension and force–velocity curves (Rome, '94).

Maintaining uniform strain is a fundamental problem in the segmented axial musculature of fishes and salamanders. Many studies have shown that the bodies of most fishes bend like a simple, homogeneous beam during swimming (e.g., Coughlin et al., '96; Katz et al., '99), and beam-like behavior dictates that the longitudinal strain (ε_x) required for a given body curvature increases with mediolateral distance from the neutral axis of bending (Katz et al., '99). Therefore, if muscle fibers are oriented longitudinally, the superficial fibers must shorten by a much greater amount than fibers near the midline and strain will not be uniform.

However, the white muscle fibers in fishes, which make up the majority of the axial muscle mass, are not oriented longitudinally and exhibit substantial architectural complexity. These fibers attach to connective tissue sheets (myosepta) that are arranged in a series of

Grant sponsor: NSF; Grant number: 0629372; Grant sponsor: US National Science Foundation; Grant number: 9875245 and 0316174.
*Correspondence to: M. Azizi, Department of Ecology and Evolutionary Biology, Brown University, 80 Waterman Street, Providence, RI 02912. E-mail: manny_azizi@brown.edu

†Present address: Department of Ecology and Evolutionary Biology, Brown University, Providence, RI 02912.
Received 24 July 2006; Revised 31 October 2006; Accepted 7 November 2006
Published online 26 January 2007 in Wiley InterScience (www.interscience.wiley.com). DOI: 10.1002/jez.a.358.

nested cones (Westneat et al., '93; Gemballa et al., 2003). The fibers are oriented such that their trajectories have both dorsoventral (α) and mediolateral (ϕ) components (Alexander, '69; Gemballa and Vogel, 2002). Segmented muscle architecture theory predicts that when fibers are oriented obliquely, the muscle fiber strain will be smaller than the longitudinal strain, i.e., $\varepsilon_f < \varepsilon_x$ (Alexander, '69; Brainerd and Azizi, 2005). The decrease in the fiber strain required to produce a given longitudinal strain results from fiber rotation, which amplifies the effect of fiber shortening and increases segment shortening velocity. The effect of muscle architecture on the strain patterns can be described by an architectural gear ratio (AGR), defined as the ratio of longitudinal strain to muscle fiber strain ($AGR = \varepsilon_x/\varepsilon_f$). The AGR is predicted to increase with increasing initial muscle fiber angle, and also to depend on the direction and magnitude of muscle bulging (Azizi et al., 2002; Brainerd and Azizi, 2005).

Alexander ('69) hypothesized that variation in white muscle fiber angles from medial to lateral in fishes may counteract the effect of distance from the neutral axis, thereby producing more uniform fiber strain across the span of the fish. This uniform strain hypothesis is supported by a study of fiber strain in frozen carp (Rome and Sosnicki, '91), but it is difficult to test in live fishes. A number of studies have used sonomicrometry to measure longitudinal strain in the red musculature during swimming (e.g., Coughlin et al., '96; Katz et al., '99; Wakeling and Johnston, '99), but it is technically more difficult to measure white fiber strain directly because the crystal pairs must be aligned along the three-dimensional trajectory of fibers. A few studies have measured superficial white fiber strain with sonomicrometry (Franklin and Johnston, '97; James and Johnston, '98; Wakeling and Johnston, '99), and one such study was designed to test Alexander's uniform strain hypothesis by measuring the ε_f of fibers with varying angles (α and ϕ) and distances (z) from the vertebral axis (Ellerby and Altringham, 2001). This latter study found that fiber strain is more uniform than would be expected if α and ϕ did not vary with mediolateral position, but that ε_f is still smaller near the vertebral column than at the periphery, indicating that the oblique orientations of the fibers are not quite sufficient to compensate for differences in z (Ellerby and Altringham, 2001).

A difficulty with studying the relationship between muscle fiber angle and fiber strain in fishes is that many fibers are angled in both the dorsoventral (α) and mediolateral (ϕ) directions. When $\phi > 0$, the effects of ϕ and z on ε_f are combined because z varies along the length of each fiber, and the magnitude of that variation is a function of ϕ. This complexity has made it difficult to quantify the relative importance of muscle fiber angle and mediolateral position in determining the strain patterns of muscle fibers during swimming.

To avoid the complex relationship between ϕ and z, we have chosen to study the segmented hypaxial musculature of an aquatic salamander, *Siren lacertina*, in which ϕ is approximately zero and α is approximately constant within each segment (Fig. 1A; Simons and Brainerd, '99). The distance to the neutral axis of bending is greater for the external oblique (EO) muscle layer than for the internal oblique (IO) layer (Fig. 1), and the resultant increase in the EO longitudinal strain is predicted by $\varepsilon_{EO} = \varepsilon_{IO}(z_{EO}/z_{IO})$, in which ε_{EO} and ε_{IO} are the strains and z_{EO} and z_{IO} are the distances from the neutral axis of the EO and IO layers, respectively. However, α in the EO is higher than α in the IO (Fig. 1), and this higher initial fiber angle may, or may not, produce uniform fiber strain in the two layers by providing the correct offset for the greater z of the EO.

In the present study, we use sonomicrometry of the EO and IO in *S. lacertina* during swimming to test two hypotheses: (1) higher initial α will result in a larger AGR (as predicted by the segmented muscle model in Brainerd and Azizi, 2005); and (2) variation in mediolateral position is counteracted by differences in AGR, resulting in uniform fiber strain and shortening velocities in the EO and IO during swimming. We then compare empirical differences in fiber strain with the variation that would be predicted if the two layers were either the same distance from the neutral axis or had the same fiber angle.

MATERIALS AND METHODS

Experimental animals

Four adult *S. lacertina* (Linnaeus) ranging in total length from 39.5 to 45.5 cm were purchased from a commercial herpetological vendor. Each individual was housed in a separate aquarium (51 cm × 26 cm × 32 cm), which was half filled with reverse osmosis purified water and maintained at $22 \pm 1^{\circ}$C. All animal care and experimental protocols used in this study were approved by the

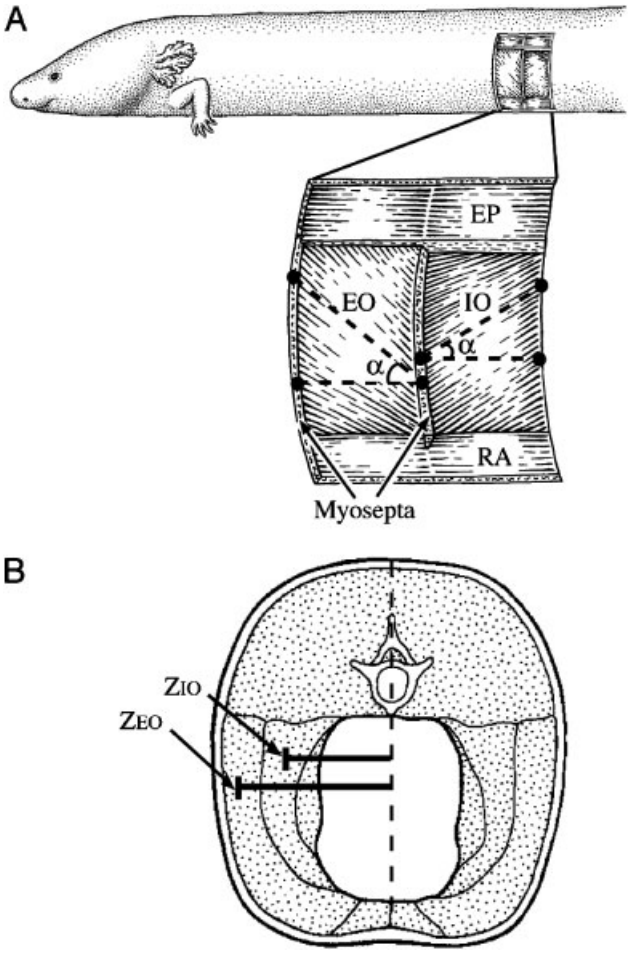

Fig. 1. (**A**) Lateral view of the external oblique (EO) and internal oblique (IO) muscle layers of *Siren lacertina*. The two hypaxial muscle layers are exposed from superficial to deep in the cranial to caudal direction. Angled muscle fibers attach to myosepta, which define the boundaries of each myomere. The approximate locations of sonomicrometry implants are shown for each layer (black circles). Muscle fiber angles (α) are defined as the absolute value of the acute angle relative to the salamander's longitudinal axis. (**B**) Transverse section of *S. lacertina* highlighting the difference in the distance (z) of the EO and IO layers from the neutral axis of bending (dashed line). Abbreviations: EO, external oblique; IO, internal oblique; RA, rectus abdominis; EP, epaxial musculature. Modified from Simons and Brainerd ('99).

University of Massachusetts Institutional Animal Care and Use Committee.

Morphological measurements

Muscle fiber angle in the hypaxial muscle layers of salamanders varies substantially among different individuals of the same species (Simons and Brainerd, '99). Therefore we measured α and muscle fiber length in vivo in anesthetized salamanders several weeks before conducting the sonomicrometry measurements. Salamanders were anesthetized by immersion in a $1\,g\,l^{-1}$ solution of buffered tricaine methanesulfonate (MS 222). Total length and snout–vent length were measured with a ruler. To measure the muscle fiber angles and fiber lengths, an incision was made in the skin so that muscle fibers from the EO layer were visible. This most superficial layer was photographed with a Nikon, Coolpix 990 digital camera mounted on a Nikon, SMZ-U dissecting microscope (Nikon Corp., Melville, NY). The muscle fibers of the EO were then spread apart and muscle fibers from the IO were photographed. Muscle fiber angle ($\pm 0.5^{\circ}$) and fiber length (± 0.2 mm) were each measured five times from the digital images of the two hypaxial layers using Image-J software (v.1.31, http://rsb.info.nih.gov/ij/). All muscle fiber angles are expressed as the absolute values of the acute angles defined relative to the longitudinal axis of the salamander (Fig. 1). To minimize the effect of this surgery on in vivo strain patterns, all morphological measurements were taken from the right side and sonomicrometry experiments were conducted on the left side of the salamander.

Sonomicrometry

Sonomicrometry was used to quantify longitudinal segment strain and muscle fiber strain in the EO and IO muscles during steady swimming. To minimize surgical trauma to the myomere of interest, separate sonomicrometry experiments were conducted on the EO and IO of each individual. Each salamander was allowed a minimum of 5 weeks to recover between experiments on each hypaxial muscle. The period of recovery allowed experiments to be conducted on both muscle layers of the same myomere.

Salamanders were anesthetized by immersion in a buffered solution of MS222 ($1\,g\,l^{-1}$). Sonomicrometry experiments were performed in the caudal region of the abdomen at the 27th myomere ($\sim$0.7TL). This longitudinal position was selected as the surgical site because in this region the hypaxial myomeres and myosepta are roughly planar, and both layers are active during steady swimming (Fig. 2; Brainerd and Azizi, 2005). Piezoelectric crystals (1 mm diameter) were purchased from Sonometrics Corp. (Toronto, Canada) and surgically implanted in the hypaxial musculature. Small incisions (approximately 5 mm) in

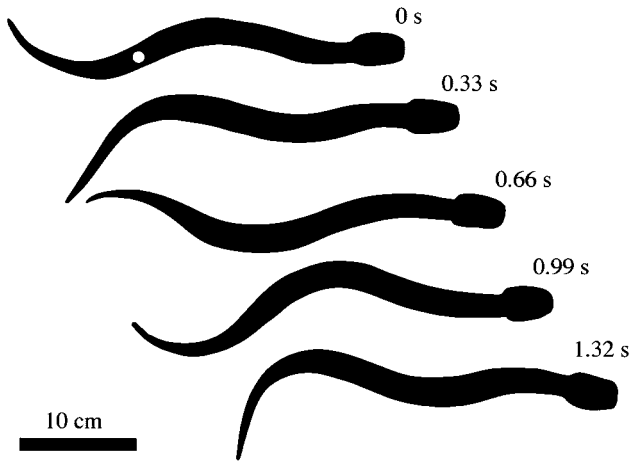

Fig. 2. Undulatory swimming kinematics of *Siren lacertina*. A representative swimming sequence is shown in dorsal view. Silhouettes are redrawn from selected video frames at 0.33 sec intervals (10 video frames). The white spot represents the location of the sonomicrometry implants.

the two adjacent myomeres were used to gain access to each muscle layer. The tips of the crystals were then pushed through small incisions in the myosepta (1 mm) into the myomere of interest, and the leads were sutured tightly to both the myosepta and the skin (the crystals themselves were embedded in the EO and IO musculature). In both layers, the crystals were arranged into a triangle such that a pair of crystals was oriented obliquely along the muscle fiber trajectory and a pair of crystals was oriented longitudinally across a myomere (Fig. 1). The transducer leads were secured to myosepta at the anterior and posterior boundaries of the myomere using 6.0 silk suture. Crystal leads were also sutured to the skin at multiple locations to prevent motion artifact during swimming. The position of the crystals was confirmed at the end of each experiment to ensure that the transducers had not moved during the course of the experiment.

The salamanders were given approximately an hour to recover from the anesthetic. During the recovery period, a TRX-6 sonomicrometer (Sonometrics Corp.) was used to measure the distances between the crystals while the body of the salamander was held straight. These measurements provided the resting lengths (L_r) of the fibers and the myomere, which are necessary for the conversion of instantaneous lengths measured by the sonomicrometer to muscle fiber strain and longitudinal strain. These measurements also allowed us to confirm signal quality and adjust sensitivity in all crystal pairs to ensure the best possible signal.

Swimming data were collected in an aquatic trackway (260 cm × 60 cm × 33 cm) filled to a height of 15 cm with water, and maintained between 21°C and 23°C. Swimming bouts were elicited by touching the tip of the salamander's tail or were initiated spontaneously by the salamander. Instantaneous distances between the crystals were collected at 250 samples sec^{-1}. Raw data files were then converted to ASCII format and exported to Sonoview (v. 3.1.4) for post-processing. Analysis was limited to swimming sequences with a minimum of four complete tail beat cycles. Trials with rapid shifts in length (level shifts), resulting from shifts in the triggering location of the transducers were also discarded. The sonomicrometry traces for each swimming sequence were smoothed using a running average algorithm (with a five point window), and raw distance measurements were converted to percent strains. These smoothed traces were then used to quantify the maximum muscle fiber strain and longitudinal strain for each tail beat. All shortening events are defined as negative strain and lengthening events as positive strain.

One potential source error associated with sonomicrometry measurements is an offset in length resulting from changes in the speed of sound through the epoxy housing of the piezoelectric crystals (Olson and Marsh, '98). To quantify this source of error we mounted a pair of 1 mm crystals on digital calipers and measured the offset in lengths reported by the sonomicrometer. We find that the average magnitude of this error is approximately 0.41 mm. This offset results in a maximum error of 6% in the reported strain values and less than 5% for most measurements. However, since both longitudinal strains and fiber strains have a similar offset error the reported values of AGR are unaffected.

Axial kinematics

Longitudinal segment strain (ε_x) data from the sonomicrometry experiments were used to quantify the magnitude and rate of axial bending during undulatory swimming at the site of the implants. Axial curvature (κ) was estimated using simple beam theory in which $\kappa = -\varepsilon_x/z$ and z is the distance of the sonomicrometry implants from the vertebral column (neutral axis of bending). For the purposes of this calculation, proportional rather than percent values of segment strain were

used. Similar calculations have been used previously to predict fiber strain in the red musculature of fishes based on axial curvature during swimming (e.g., Coughlin et al., '96; Katz et al., '99). The rate of change of the curvature ($\Delta\kappa/\Delta t$) was then used to quantify bending rate during swimming bouts.

To examine whether axial bending in *S. lacertina* can be accurately characterized by simple beam theory, we combined our sonomicrometry experiments with video motion analysis. Swimming bouts were filmed in dorsal view using a Sony DCR-VX2000 camcorder (Sony Corp., New York, NY, USA). Sonomicrometry traces were superimposed onto video recordings using a TelevEyes/Pro video overlay box (Digital Vision Inc., USA). The synchronized video was recorded on a Sony GV-D900 digital video recorder (Sony Corp.). This process allowed us to correlate the timing of swimming movements with sonomicrometry measurements. Video images were used to create midlines of the swimming salamander. The coordinates describing the midline were fitted with a polynomial (u), which was used to solve for axial curvature (cm^{-1}) at the location of the sonomicrometry implants (x) using the following equation (Katz and Shadwick, 2000):

$$\kappa(x) = u''(x)/(1 + u'(x)^2)^{3/2} \quad (1).$$

For each tail beat, maximum curvature and maximum bending rate were quantified on the same side of the body as the sonomicrometry implants. Mean maximum curvature and mean maximum bending rates were then quantified for each locomotor bout and used in our statistical analyses to account for potential kinematic differences between experiments and among individuals.

Statistical analyses

To quantify AGR for the IO and EO in each of the four individual study animals, the maximum longitudinal strain of each tail beat was plotted against the maximum muscle fiber strain of that tail beat. An orthogonal regression assuming equal error in the x and y variables (major axis regression) was then performed (SPSS Inc., Chicago, IL). The major axis regression lines were forced through the origin because without muscle fiber shortening, no longitudinal shortening would be expected. The slope of this regression was then used to estimate the AGR at the measured muscle fiber angle of the muscle layer in the specific individual salamander. Pearson-product correlation coefficients (R) and 95% confidence intervals of the slope were used to estimate the variance of our AGR measurements. To examine the effect of the fiber angle on AGR, separate least-squares regressions were performed on data from the IO and EO. These regressions were forced through a y-intercept of 1, which represents the condition where longitudinal shortening equals fiber shortening.

To compare muscle fiber strain in the EO and IO layer of each individual, the average fiber strain for the tail beats in one swimming bout were calculated and adjusted for the mean axial curvature in that bout. Similarly, to compare muscle fiber shortening velocity in the two hypaxial layers of each individual, the average shortening velocity for the tail beats in one swimming bout were calculated and adjusted for the mean bending rate in that bout. For each individual, adjusted means (least-squares means) along with 95% confidence intervals were calculated for each layer using SuperAnova (v. 1.11; Abacus Concepts Inc., Berkeley, CA). A Student's t-test was performed on the adjusted means to compare the strains and shortening velocities of the IO and EO in each individual. This analysis was used to account for potential variation in axial kinematics during the two experiments conducted on the same individual.

RESULTS

Muscle architecture

In the abdominal region, the hypaxial myomeres of *S. lacertina* are approximately planar and are separated by transverse planar myosepta (Fig. 1). Each hypaxial myomere spans a single vertebral segment and is approximately 7 mm long (longitudinal distance between adjacent myosepta) in the individuals used in this study (Table 1). Muscle fibers of the EO and IO span the length of a myomere and attach to adjacent myosepta at oblique angles (α) relative to the longitudinal axis. The fibers of the EO are oriented from craniodorsal to caudoventral and the fibers of the IO are oriented from cranioventral to caudodorsal (Fig. 1). Similar to previous descriptions of the muscle architecture of hypaxial myomeres in salamanders (Simons and Brainerd, '99), we find substantial interindividual variation in α. In the individuals used in this study, α in the EO ranged from 36.5° to 43° and α in the IO ranged from 17° to 23° (Table 1).

TABLE 1. Morphometric and muscle architecture data

			α (deg)			Fiber length (mm)		*z* (mm)	
Individual	TL (cm)	SVL (cm)	IO	EO	Segment length (mm)	IO	EO	IO	EO
1	40.3	27.5	17°	43.0°	6.75	7.05	9.22	8.5	11.5
2	42.3	31.4	23°	40.5°	7.35	7.95	9.65	9.5	13.0
3	39.5	27.0	21°	39.0°	6.15	6.60	7.91	7.5	11.5
4	45.5	29.9	19°	36.5°	7.15	7.55	8.90	9.5	14.5

EO, external oblique layer; IO, internal oblique layer.

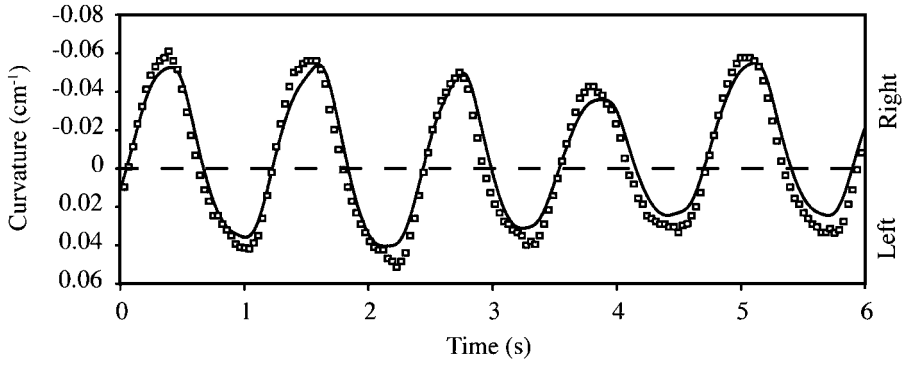

Fig. 3. Two estimates of axial curvature during undulatory swimming. Curvature was calculated (Eq. (1)) by generating midlines of the salamander from video images and solving for localized curvature (open squares). Curvature was also calculated by using longitudinal strain data from sonomicrometry combined with beam theory (solid line). A single swimming bout consisting of five complete tail beat cycles is shown. We have defined positive curvature to coincide with muscle shortening on the side of the sonomicrometry implants. The two methods provide similar estimates of the magnitude and phase of axial curvature during undulatory swimming, indicating that axial bending in this salamander can be accurately characterized by simple beam theory.

Axial kinematics

S. lacertina uses an anguilliform mode of undulatory swimming (Fig. 2). During swimming, waves of axial bending generally begin in the anterior third of body and propagate posteriorly. These axial waves tend to have relatively large amplitudes and small wavelengths such that an entire wave may be present on the body at any point during a tail beat (Fig. 2). In this study, we limit our quantitative kinematic analysis to the magnitude and rate of axial bending during undulatory swimming in order to interpret the strain patterns measured by sonomicrometry. For a detailed analysis of the swimming kinematics of *Siren*, refer to Gillis ('97).

We compared axial curvature quantified using longitudinal strains from sonomicrometry with curvature values based on video motion analysis. We find strong agreement between the values of curvature measured using these two methods. A time-series trace highlights the similarity in the magnitude and phase of the two estimates of axial curvature (Fig. 3). These results indicate that muscle fiber strain and the resultant axial muscle forces produce localized axial bending at the same body position, and therefore axial bending in *S. lacertina* can be accurately characterized by beam theory.

Strain patterns and architectural gear ratio

Our sonomicrometry results indicate that the magnitude of muscle fiber strain in both the EO and IO layers is smaller than the corresponding longitudinal strain at the same distance from the neutral axis during undulatory swimming (Fig. 4). These findings show that muscle fiber strain is amplified and that the angled muscle fibers of the EO and IO have AGRs that are greater than one. To quantify AGR, we plotted muscle fiber strain against longitudinal segment strain recorded from each hypaxial muscle layer in each individual

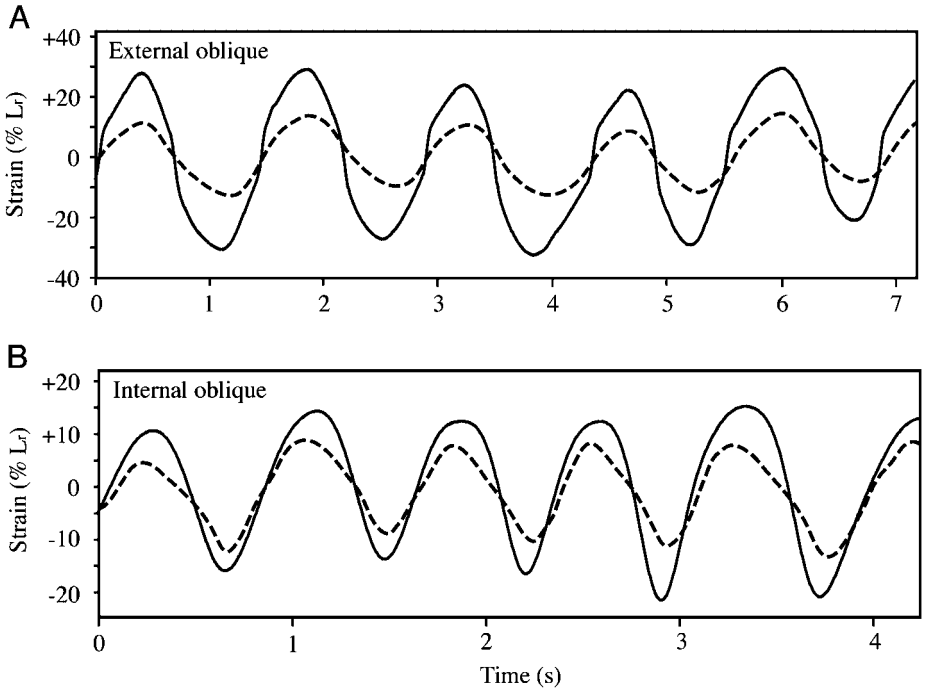

Fig. 4. Sonomicrometry traces of muscle longitudinal strain (solid lines) and muscle fiber strain (dashed lines). (**A**) External oblique during a representative swimming bout. (**B**) Internal oblique layer during a different representative swimming bout. In both muscle layers longitudinal strain is greater than muscle fiber strain, indicating that gear ratio is greater than 1. L_r = resting length.

(Fig. 5), and the slopes of these regressions were used to quantify the AGR. Then we used the differences in α among individuals and between the EO and IO to plot AGR vs. α (Fig. 6). Data from the IO and EO were fit with least-squares regression lines, which were forced through a *y*-intercept of 1. Our results indicate that AGR increases significantly with increasing fiber angle in both the IO ($P = 0.0009$) and EO ($P = 0.016$).

Muscle fiber strain and shortening velocity

To assess whether muscle fiber strain is uniform in the EO and IO layers of each individual, we compared the mean maximum fiber strain of all undulatory swimming bouts in each layer. However, since we did not control the speed of swimming bouts, mean muscle fiber strain data were adjusted for potential differences in the magnitude of axial bending (curvature), which was included in the analysis as a covariate. A comparison of the adjusted (least-squares) mean strain data from the two hypaxial layers of each individual is shown in Figure 7A. Based on Student's *t*-tests performed, we find that despite substantial differences in α and z, fiber strain is not significantly different in the EO and IO of three individuals (Ind. 1, $P = 0.174$; Ind. 2, $P = 0.105$; Ind. 3, $P = 0.153$). In the fourth individual, EO fiber strain is higher than IO strain, as would be predicted by the greater distance of the EO from the neutral axis of bending ($P < 0.0001$).

Similar to our analysis of the magnitude of muscle fiber strain described above, we also compared the shortening velocity of fibers in the EO and IO of each individual. Since we did not control the speed of swimming bouts, shortening velocity data were adjusted for potential differences in the rate of axial bending, which was included in the analysis as a covariate. A comparison of the adjusted (least-squares) mean shortening velocity data ($\%L_r\,sec^{-1}$) from the two hypaxial layers of each individual is shown in Figure 7B. Based on Student's *t*-tests performed, we find that shortening velocity is not significantly different in the EO and IO of three individuals (Ind. 1, $P = 0.168$; Ind. 2, $P = 0.059$; Ind. 3, $P = 0.08$), but the shortening velocity of the EO is higher than the IO in the fourth individual ($P < 0.0001$).

The empirical differences in the overall mean fiber strain of the EO and IO can be compared to theoretical cases in which the EO and IO are either

located at same distance from the neutral axis ($\Delta z = 0$) or have the same initial fiber angle ($\Delta\alpha = 0$). The theoretical calculations are based on the average difference in the IO and EO's distance from the neutral axis and the average AGR for each layer (Fig. 8). In the fist condition shown ($\Delta z = 0$), the ratio of fiber strains in the two layers is calculated only from their relative distance from the neutral axis using beam theory. In the second condition ($\Delta\alpha = 0$), the ratio of fiber strains is calculated only from the average gear ratio of each layer. This comparison highlights the effects of z and α on the relative magnitude of fiber strain and indicates that in our measurements from *S. lacertina*, the variation in muscle fiber angle acts to counteract variation in z and thereby to produce more uniform fiber strain during swimming (Fig. 8).

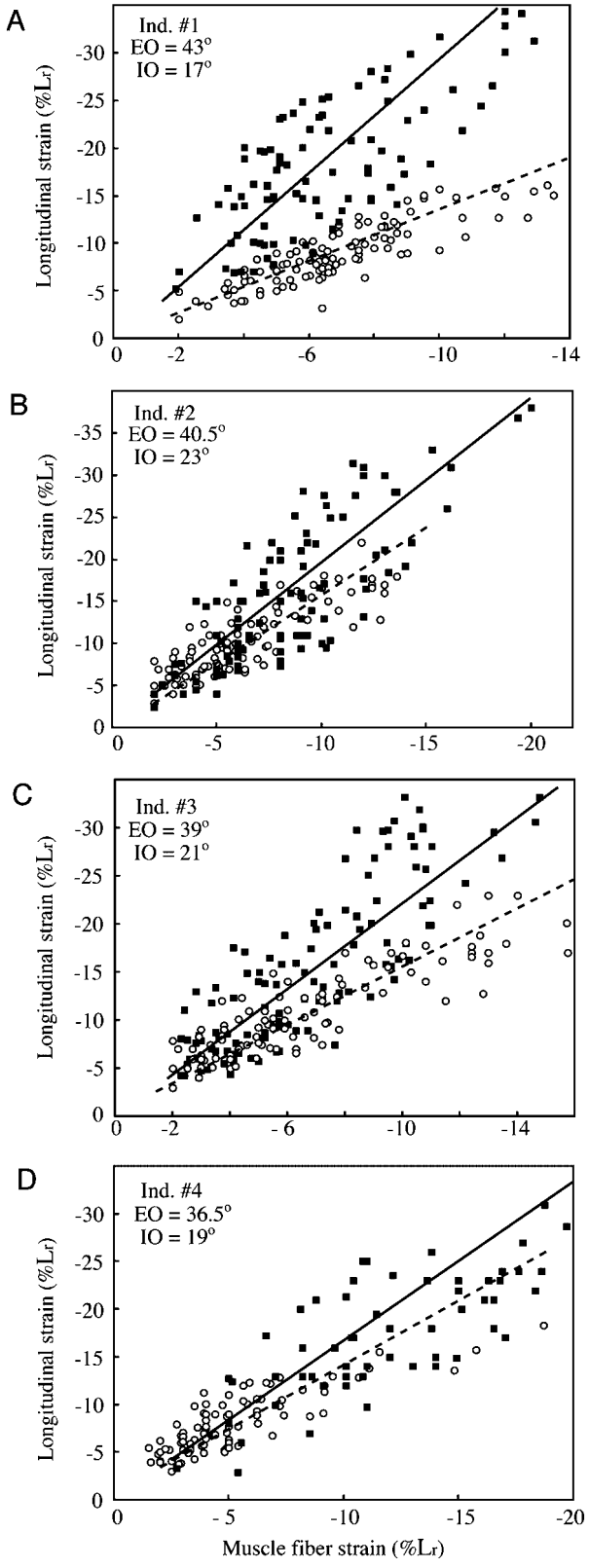

Fig. 5. Muscle fiber strain vs. longitudinal strain during swimming for four individuals with varying initial muscle fiber angles in the external oblique (EO) and internal oblique (IO) muscle layers. The individual points are the peak shortening (most negative strain) from each tail beat. Data from the EO (solid squares) and IO (open circles) are fitted with reduced major axis regression lines (EO solid, IO dashed), which have been forced through the origin. The slopes from these regression lines are used estimate architectural gear ratio at a given muscle fiber angle. (**A**) Individual 1: EO slope = 2.78 ± 0.079 ($R = 0.73$); IO slope = 1.31 ± 0.024 ($R = 0.87$). (**B**) Individual 2: EO slope = 1.92 ± 0.057 ($R = 0.82$); IO slope = 1.61 ± 0.043 ($R = 0.84$). (**C**) Individual 3: EO slope = 2.34 ± 0.062 ($R = 0.84$); IO slope = 1.56 ± 0.039 ($R = 0.84$). (**D**) Individual 4: EO slope = 1.48 ± 0.032 ($R = 0.76$); IO slope = 1.46 ± 0.059 ($R = 0.83$). Error terms are standard errors of the slope; R is the Pearson-product correlation coefficient. L_r = resting length.

DISCUSSION

Homogeneity of muscle fiber strain and shortening velocity

In this study we find that AGR increases with increasing muscle fiber angle, as predicted by mathematical models of segmented and pinnate muscle architecture (Benninghoff and Rollhäuser, '52; Alexander, '69; Gans, '82; Otten, '88; Brainerd and Azizi, 2005). We also find that variation in mediolateral position is counteracted by the observed differences in AGR, resulting in similar fiber strains and shortening velocities in the EO and IO of *S. lacertina* during swimming (Fig. 7). We conclude that the architectural differences between the EO and IO act to minimize variation in muscle fiber strain and shortening velocity in fibers that are located at different distances from the neutral axis of bending.

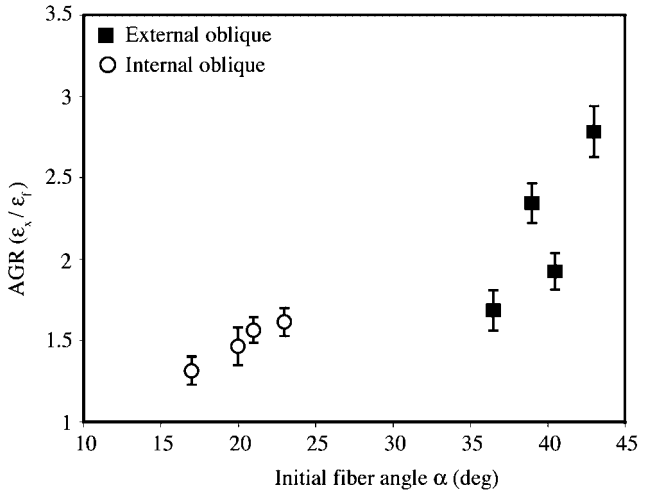

Fig. 6. Architectural gear ratio of external oblique (EO) and internal oblique (IO) muscle layers from four individuals with varying initial muscle fiber angles. Slopes of reduced major axis regressions (Fig. 5) were used to estimate AGR (±95% CI). Data from the EO are shown as closed squares and data from the IO are shown as open circles; each point represents one individual (±95% CI of the slope).

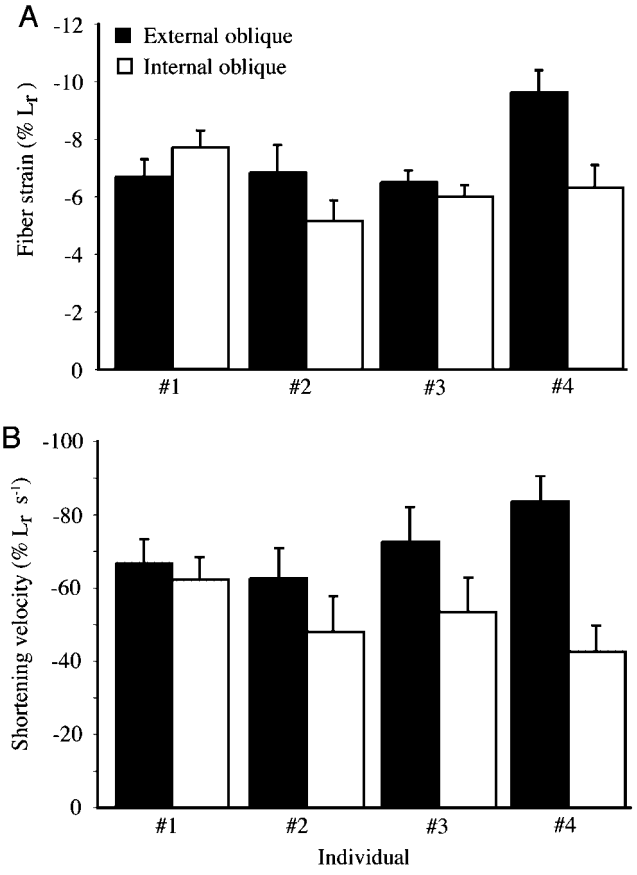

Fig. 7. Muscle fiber strain and shortening velocity in the external oblique (EO) and internal oblique (IO) layers. (**A**) Adjusted (least-squares) mean muscle fiber strain in the EO (black) and IO (white) of each individual. All swimming sequences from each individual have been pooled and means are adjusted for differences in localized axial curvature. (**B**) Adjusted (least-squares) mean fiber shortening velocity in the EO (black) and IO (white) of each individual. All swimming sequences from each individual have been pooled and means are adjusted for differences in the rate of axial bending. Error bars are 95% confidence limits of the means. L_r = resting length.

It has previously been hypothesized that muscle fibers recruited for a given task will have similar strains and shortening velocities in order to function within the mechanical constraints of the vertebrate sarcomere (Calow and Alexander, '73; Rome, '94). Such predictions are based on the fact that optimal tension can only be generated over a limited range of muscle fiber strains where myofilament overlap can be maximized. Similarly, peak power is only possible over the small range of shortening velocities at which cross-bridge formation can be maximized. Our results suggest that one potential solution for circumventing the length–tension and force–velocity constraints of sarcomeres is through architectural variation.

Inter-individual variation in muscle architecture

A previous survey of lateral hypaxial muscle architecture in salamanders found substantial interindividual (intraspecific) variation in every species examined (Simons and Brainerd, '99). Among the four *S. lacertina* individuals in our study, the resting fiber angles ranged from 36.5° to 43.0° in the EO and from 17.0° to 23.0° in the IO. Our empirical measurements of AGR show that this anatomical variation causes a measurable difference in function, with AGR tending to be higher in individuals with higher initial fiber angles (Fig. 6). Individual 4 had the lowest EO angle, and the correspondingly low AGR for the EO in this individual was not sufficient to compensate for the greater distance from the neutral axis (Fig. 7). Therefore, the observed interindividual variation affected not only the AGR of each layer, but also caused markedly non-uniform strain in the EO and IO during swimming in individual 4.

Although initial muscle fiber angle is an important determinant of AGR, the magnitude of dorsoventral bulging is also expected to affect the amount of fiber rotation and the AGR (Azizi et al., 2002; Brainerd and Azizi, 2005). Interindividual

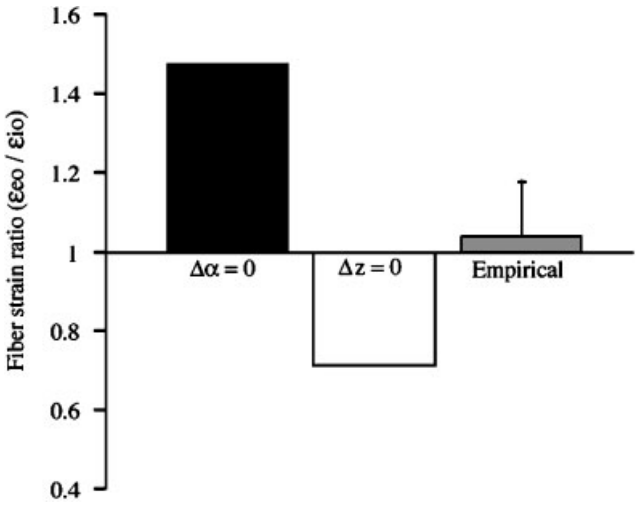

Fig. 8. The effect of fiber angle and mediolateral position on strain variation in the EO and IO. If the fiber angle in the EO and IO were equal, the measured difference in z (Table 1) would result in fiber strain being 1.5× greater in the EO (black bar). If the mediolateral position of the EO and IO were equal, the measured variation in fiber angle and AGR (Fig. 6) would result in fiber strain being 1.4× greater in the IO (white bar). These theoretical conditions are shown alongside the average ratio of fiber strain (±s.e.m.) measured during swimming (gray bar, pooled from four individuals). A value of one indicates equal strain; values greater than one indicate EO has larger strains than IO, and values less than one indicate IO has larger strains than EO.

differences in bulging may explain the measured AGRs in the two individuals with EO angles of 39.0° and 40.5°. We would expect AGR in the 40.5° EO to be slightly higher than the 39.0° EO, but instead the AGR of the 39.0° EO is substantially higher than that of the 40.5° EO (Fig. 6). One possible explanation for this unexpected result is that dorsoventral bulging is greater in the 39.0° EO, which would increase the AGR in this individual. However, the significance and/or prevalence of such interindividual variation in the dynamic architectural features of muscle remain unclear and warrant further investigation.

Gear ratio and muscle architecture

Broadly defined, a gear ratio describes the relative force and displacement components of any mechanical system. In musculoskeletal biomechanics, gear ratios have commonly been used to describe the relationship between the in-levers and out-levers of muscle–joint complexes (e.g., Biewener, '89; Carrier et al., '98; Roberts and Marsh, 2003; Gregersen and Carrier, 2004). In the distal joints of tetrapods, a high gear ratio produces a velocity advantage and is a function of the moment arms of both the muscle (in-lever) and the ground reaction forces (out-lever) about a joint's center of rotation. Similarly, in the axial musculature of fishes and salamanders, the distance from the neutral axis is effectively a gearing factor that increases the velocity of body bending and decreases the bending moment when muscle fibers are located close to the neutral axis.

In segmented and pinnate muscles, an analogous relationship of the gearing between muscle fiber shortening and the shortening of the whole muscle can be described by the AGR (Brainerd and Azizi, 2005). In the AGR, muscle fiber shortening represents the in-lever and whole muscle shortening represents the out-lever.

Just as a muscle's in-lever can be used to predict the whole muscle shortening required to produce a given joint movement, AGR can predict the fiber strain required for a given amount of muscle shortening. Therefore, the combined effects of these two levels of gearing determine the relationship between the length changes of a fiber and the movement of a joint.

The cumulative effect of AGR and moment arms is exemplified by our result that the fibers of the EO and IO muscle layers undergo similar strains and shortening velocities during swimming in *S. lacertina*. While the two levels of gearing counteract one another in the hypaxial musculature of salamanders, the cumulative effects of AGR and moment arms could also function synergistically to amplify the velocity or force output of specialized musculoskeletal systems.

Incorporation of the gearing at both the architectural and moment arm levels in studies of muscle function is complicated by the fact that both features change dynamically throughout a muscle contraction. Dynamic gearing in muscle–tendon units can result from changes in the orientation of the ground reaction force (Carrier et al., '94, '98; Roberts and Marsh, 2003), and/or changes in the muscle moment arms with changing joint angle (Wretenberg et al., '96). Similarly, AGR changes dynamically because it depends on the magnitude of fiber rotation, which in turn depends on how the muscle changes shape (bulges) during a contraction (Brainerd and Azizi, 2005). The dynamic nature of AGR suggests that architectural features are muscle- and even task-specific and cannot simply be determined from cadaver-based measurements of fiber angle. Therefore, the use of generalized correction

factors to account for pinnation angle may lead to inaccurate results. However, advances such as sonomicrometry and ultrasound imaging now make it possible to measure AGR directly and should allow studies of muscle function to integrate dynamic gearing both within the muscle and at the joint to characterize more accurately the relationship between muscle fiber strain and external movement.

ACKNOWLEDGMENTS

This work was conducted as part of the requirements for a doctoral degree in Organismic and Evolutionary Biology from the University of Massachusetts, Amherst. The authors thank Willy Bemis, Graham Caldwell, and Steve McCormick for guidance during the early stages of this project and for helpful comments on early drafts of this manuscript. They also thank Tom Roberts, Steve Gatesy, Dale Ritter, Frank Nelson, and Jonna Hamilton for commenting on this manuscript.

LITERATURE CITED

Alexander RM. 1969. Orientation of muscle fibers in the myomeres of fishes. J Mar Biol Assoc UK 49:263–290.

Azizi E, Gillis GB, Brainerd EL. 2002. Morphology and mechanics of myosepta in a swimming salamander (*Siren lacertina*). Comp Biochem Physiol A 133:967–978.

Benninghoff A, Rollhäuser H. 1952. Zur Inneren Mechanik Des Gefiederten Muskels. Pflügers Arch Gesamte Physiol Menschen Tiere 254:527–548.

Biewener AA. 1989. Scaling body support in mammals—limb posture and muscle mechanics. Science 245:45–48.

Brainerd EL, Azizi E. 2005. Muscle fiber angle, segment bulging and architectural gear ratio in segmented musculature. J Exp Biol 208:3249–3261.

Calow LJ, Alexander RM. 1973. A mechanical analysis of a hind leg of a frog (*Rana temporaria*). J Zool Lond 171: 293–321.

Carrier DR, Heglund NC, Earls KD. 1994.Variable gearing during locomotion in the human musculoskeletal system. Science 265:651–653.

Carrier DR, Gregersen CS, Silverton NA. 1998 Dynamic gearing in running dogs. J Exp Biol 201:3185–3195.

Coughlin DJ, Valdes L, Rome LC. 1996. Muscle length changes during swimming in scup: sonomicrometry verifies the anatomical high-speed cine technique. J Exp Biol 199: 459–463.

Ellerby DJ, Altringham JD. 2001. Spatial variation in fast muscle function of the rainbow trout *Oncorhynchus mykiss* during fast-starts and sprinting. J Exp Biol 204: 2239–2250.

Franklin CE, Johnston IA. 1997. Muscle power output during escape responses in an Antarctic fish. J Exp Biol 200: 703–712.

Gans C. 1982. Fiber architecture and muscle function. Excer Sport Sci Rev 10:160–207.

Gemballa S, Vogel F. 2002. Spatial arrangement of white muscle fibers and myoseptal tendons in fishes. Comp Biochem Physiol A—Mol Integr Physiol 133:1013–1037.

Gemballa S, Ebmeyer L, Hagen K, Hannich T, Hoja K, Rolf M, Treiber K, Vogel F, Weitbrecht G. 2003. Evolutionary transformations of myoseptal tendons in gnathostomes. Proc R Soc Lond B Biol 270:1229–1235.

Gillis GB. 1997. Anguilliform locomotion in an elongate salamander (*Siren intermedia*): effects of speed on axial undulatory movements. J Exp Biol 200:767–784.

Gregersen CS, Carrier DR. 2004. Gear ratios at the limb joints of jumping dogs. J Biomech 37:1011–1018.

James RS, Johnston IA. 1998. Scaling of muscle performance during escape responses in the fish *Myoxocephalus scorpius* L. J Exp Biol 201:913–923.

Katz SL, Shadwick RE. 2000. In vivo function and functional design in steady swimming fish muscle. In: Herzog W, ed: Skeletal muscle mechanics; from mechanisms to function. New York: Wiley. p 1–27.

Katz SL, Shadwick RE, Rapoport HS. 1999. Muscle strain histories in swimming milkfish in steady and sprinting gaits. J Exp Biol 202:529–541.

Olson JM, Marsh RL. 1998. Activation patterns and length changes in hindlimb muscles of the bullfrog *Rana catesbeiana* during jumping. J Exp Biol 201:2763–2777.

Otten E. 1988. Concepts and models of functional architecture in skeletal muscle. Exerc Sport Sci Rev 16:89–137.

Roberts TJ, Marsh RL. 2003. Probing the limits to muscle-powered accelerations: lessons from jumping bullfrogs. J Exp Biol 206:2567–2580.

Rome LC. 1994. Mechanical design of the fish muscular system. In: Maddock L, Bone Q, Rayner JMV, editors. Mechanics and physiology of animal swimming. Cambridge: Cambridge University Press. p 75–97.

Rome LC, Sosnicki AA. 1991. Myofilament overlap in swimming carp. 2. sarcomere-length changes during swimming. Am J Physiol 260:C289–C296.

Simons RS, Brainerd EL. 1999. Morphological variation of hypaxial musculature in salamanders (Lissamphibia: Caudata). J Morphol 241:153–164.

Wakeling JM, Johnston IA. 1999. White muscle strain in the common carp and the red to white muscle gearing ratios in fish. J Exp Biol 202:521–528.

Westneat MW, Hoese W, Pell CA, Wainwright SA. 1993. The horizontal septum: mechanisms of force transfer in locomotion of scombrid fishes (Scombridae, Perciformes). J Morphol 217:183–204.

Wretenberg P, Nemeth G, Lamontagne M, Lundin B. 1996. Passive knee muscle moment arms measured in vivo with MRI. Clin Biomech 11:439–446.